Optics Letters

Selective reflection from an Rb layer with a thickness below λ/12 and applications

Armen Sargsyan,[1] Aram Papoyan,[1,*] Ifan G. Hughes,[2] Charles S. Adams,[2] and David Sarkisyan[1]

[1]Institute for Physical Research, NAS of Armenia, 0203 Ashtarak-2, Armenia
[2]Joint Quantum Centre (JQC) Durham-Newcastle, Department of Physics, Durham University, South Road, Durham DH1 3LE, UK
*Corresponding author: papoyan@ipr.sci.am

Received 22 February 2017; revised 14 March 2017; accepted 14 March 2017; posted 14 March 2017 (Doc. ID 287268); published 4 April 2017

We have studied the peculiarities of selective reflection from an Rb vapor cell with a thickness $L < 70$ nm, which is smaller than the length scale of evanescent fields $\lambda/2\pi$ and more than an order of magnitude smaller than the optical wavelength. A 240 MHz redshift due to the atom-surface interaction is observed for a cell thickness of $L = 40$ nm. In addition, complete frequency-resolved hyperfine Paschen–Back splitting of atomic transitions to four components for ^{87}Rb and six components for ^{87}Rb is recorded in a strong magnetic field ($B > 2$ kG).

OCIS codes: (020.3690) Line shapes and shifts; (300.6320) Spectroscopy, high-resolution; (300.6210) Spectroscopy, atomic.

https://doi.org/10.1364/OL.42.001476

Selective reflection (SR) of resonant optical radiation from the interface between an atomic vapor and the dielectric window of spectroscopic cells was initially observed by Wood in 1909 [1], and revisited in the 1970s when narrow-linewidth tunable cw lasers became available [2–4]. Thanks to the high-contrast sub-Doppler signal response, the SR technique became a powerful spectroscopic tool, which was successfully used, in particular, to study the van der Waals (vdW) interaction of atoms with a dielectric window of the cell manifested by a redshift of the SR frequency [5–8]. Spectroscopy with atomic vapor nanometric-thickness cells (NCs) is another technique capable of yielding information on atom-surface processes. The vdW interaction of Rb and Cs atoms confined in the NCs was studied in [9] using resonant fluorescence spectra.

Merging the SR and NC methods significantly extends their applied interest. On account of the dispersive shape of the signal, the SR from the NCs was used to lock the laser's frequency [10]. Recently, it was demonstrated that the SR from a Rb vapor NC with thickness $L \approx 370$ nm is convenient to form frequency reference of atomic transitions [11]. It was also shown that the same technique implemented for the D_1 line of Cs and 300 nm gap thickness is expedient to study the behavior of atomic transitions in a strong magnetic field [12].

In this Letter, we focus on the peculiarities of SR for the conditions when the response of a resonant medium is formed over an essentially sub-wavelength depth in an atomic vapor layer geometrically restricted by the two inner surfaces of the NC ($L < 70$ nm). For the first time, to the best of our knowledge, we have implemented a "derivative SR" (DSR) method for atomic layers with a thickness in the range of tens of nm.

The experimental arrangement is schematically sketched in Fig. 1. The collimated circularly polarized beam of a single-frequency narrow-band ($\gamma_L \sim 1$ MHz) cw external cavity diode laser with $\lambda = 795$ nm and power $P_L \sim 0.5$ mW was directed at normal incidence onto the specially fabricated Rb NC with a large aperture area of smoothly changing thickness in the range $L = 20 - 90$ nm (see the upper right inset). The thickness L was measured by an interferometric technique presented in [13]. The SR beam was carefully separated from two other beams reflected from the front and rear surfaces of the cell (see the upper left inset) and after passing through a $\lambda = 795$ nm interference filter was recorded by a photodiode (PD_{SR}).

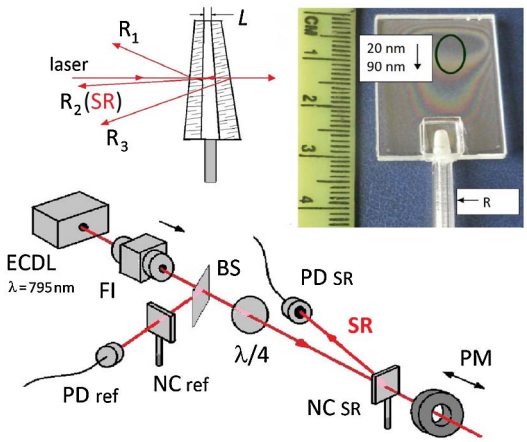

Fig. 1. Layout of the experimental setup: ECDL, cw laser; FI, Faraday isolator; BS, beam splitter; NC, Rb nanometric-thickness cell inside an oven; PM, permanent magnet; PD, photodetector; $\lambda/4$, quarter-wave plate ("SR" and "ref" denote SR and reference channels). Upper right inset, photograph of the NC; the oval marks 20–90 nm region. Upper left inset, geometry of the 3 reflected beams. The beam (SR) propagates in the direction of R_2.

A fraction of laser radiation was branched to the frequency reference unit with an auxiliary Rb NC with $L = \lambda$ (NC ref) to form a transmission spectrum exhibiting narrow velocity selective optical pumping (VSOP) resonances located exactly at atomic transition frequencies [14]. The reference signal was recorded simultaneously with the SR signal by a two-channel digital oscilloscope while linearly scanning the laser frequency across the D_1 resonance. The scanning rate was chosen to be slow enough for assuring the establishment of a steady-state interaction regime.

The necessary vapor density ($\approx 8 \times 10^{13}$ cm^{-3}) was attained by heating the cell's thin sapphire reservoir (R) containing metallic Rb to $T_R \approx 150$°C, while keeping the window temperature some 20°C higher. Note that the NC can be heated up to 450°C (see [13,14]). To study magnetic field-induced processes, a calibrated strong permanent neodymium magnet (PM) was mounted on a micrometric-step translation stage in the proximity of the cell's rear window. The B-field strength was varied by simple longitudinal displacement of the magnet.

The SR spectrum on the D_1 line $F_g = 2, 3 \rightarrow F_e = 3$ transitions of ^{85}Rb and $F_g = 1, 2 \rightarrow F_e = 2$ transitions of ^{87}Rb for the cell thickness of 67 nm and longitudinal magnetic field $B \approx 2.4$ kG is shown in Fig. 2 (upper spectrum). (Please note that in the figures the excited levels are marked by primes.) The lower lines are the derivatives of the SR signal (DSR) formed in real time by the Siglent oscilloscope. Studies of a sub-Doppler spectrum emerging in the derivative of the SR signal are presented in [11,12]. The DSR peaks labeled 1–3 and 10 belong to ^{87}Rb, and the DSR peaks 4–9 belong to ^{85}Rb (see the upper diagrams). On account of the sub-Doppler linewidth of the DSR ($\gamma_{\mathrm{DSR}} \approx 200$ MHz FWHM), all 10 transition components for $B = 2.4$ kG are spectrally well resolved. For $B = 2.7$ kG, complete frequency resolution is observed for all transition components, except overlapping peaks 3 and 6. The influence of the vdW interaction between the atoms and dielectric windows of the NC starts to feature in the spectra when $L < 100$ nm [6,7], manifested as a redshift of the SR signal frequency. This shift is clearly observable for $B = 0$, $L \approx 67$ nm, as is shown in the middle inset of Fig. 2 (see the figure caption).

The influence of the applied magnetic field on the hyperfine structure is characterized by parameter $B_0 = A_{\mathrm{HFS}}/\mu_B$, where A_{HFS} is the hyperfine coupling constant for 5S level, and μ_B is the Bohr magneton [15]. $B_0 \approx 0.7$ kG for ^{85}Rb, and $B_0 \approx 2$ kG for ^{87}Rb. When $B < B_0$ (Zeeman regime), the splitting of levels is described by the total angular momentum of the atom $\mathbf{F} = \mathbf{J} + \mathbf{I}$ and its projection m_F, where $\mathbf{J}$ is the total electron angular momentum, and $\mathbf{I}$ is the nuclear spin angular momentum. The F and m_F notation is used in the inset diagram of Fig. 2. Decoupling between $\mathbf{J}$ and $\mathbf{I}$ develops when $B \geq B_0$. F is no longer a good quantum number, and the splitting of the atomic levels is described by the projections m_J and m_I (hyperfine Paschen–Back regime) [16–18]. In this regime, four and six atomic transitions belonging to ^{87}Rb and ^{85}Rb, respectively, remain in the spectra (as is evident in Figs. 2 and 3).

The recorded DSR spectrum for $L = 50 \pm 2$ nm and $B \approx 2.15$ kG is shown in Fig. 3. For this measurement, the reservoir temperature was somewhat increased ($T_R = 165$°C) to compensate for the thickness reduction. In spite of some broadening of the DSR ($\gamma_{\mathrm{DSR}} \approx 250$ MHz), all the peaks are well resolved, except 3 and 5, which are overlapped. The inset in the upper right corner shows the $B = 0$ spectra, which clearly indicate the increase of vdW redshift to –130 MHz with respect to unperturbed atomic transitions. To estimate the frequency shift for RbD_1 line arising from the interaction of an individual atom with two dielectric windows of the cell (w1 and w2), we have plotted in the upper left inset the distance-dependent frequency shifts separately for w1: $\Delta\nu_{\mathrm{vdW}} = -C_3/z_1^3$ (curve 1), and for w2: $\Delta\nu_{\mathrm{vdW}} = -C_3/z_2^3$ (curve 2), where z_1 and z_2 are the distances of the Rb atom from w1

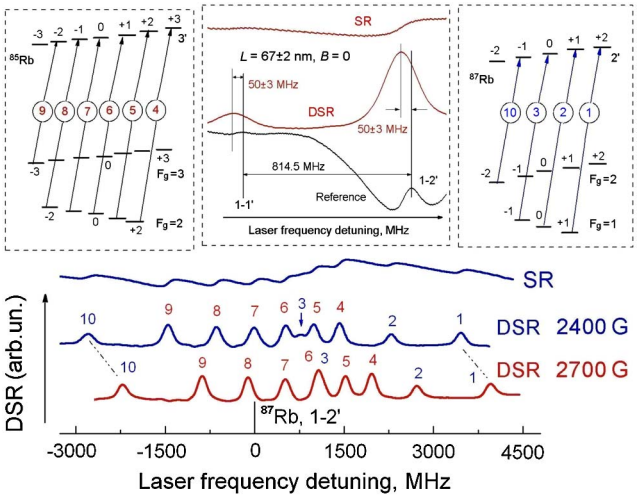

Fig. 2. SR spectrum (SR, upper line) and its derivative (DSR) for $L = 67 \pm 2$ nm, recorded at $B = 2.4$ kG (middle curve), and 2.7 kG (lower curve). For labeling, see the upper left- and right-side insets presenting σ^+-polarized transition diagrams for ^{85}Rb and ^{87}Rb, respectively. Upper middle inset, $B = 0$ spectra (from top to bottom: SR, DSR, and reference) exhibiting ~50 MHz redshift with respect to $F_g = 1 \rightarrow F_e = 1, 2$ transitions of ^{87}Rb.

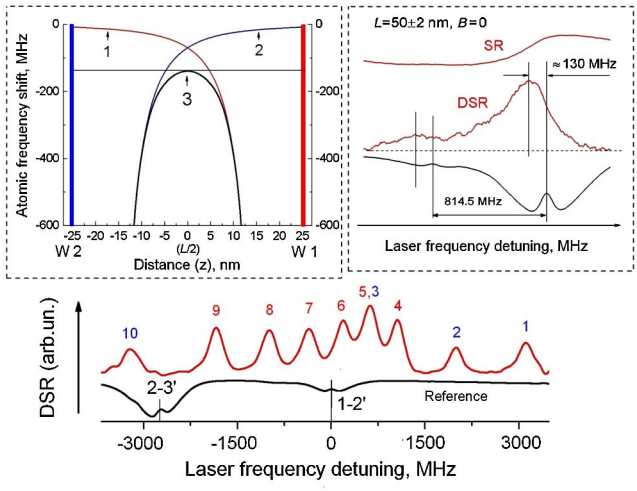

Fig. 3. Experimental DSR spectrum for $L = 50 \pm 2$ nm recorded at $B = 2.15$ kG. Upper right inset, $B = 0$ spectra (from top to bottom: SR, DSR, and reference), exhibiting –130 MHz redshift with respect to ^{87}Rb $F_g = 1 \rightarrow F_e = 1, 2$ reference frequencies. Upper left inset, the estimate of distance-dependent vdW redshift; the horizontal line tangent to an overall curve 3 marks the minimum shift value (–130 MHz).

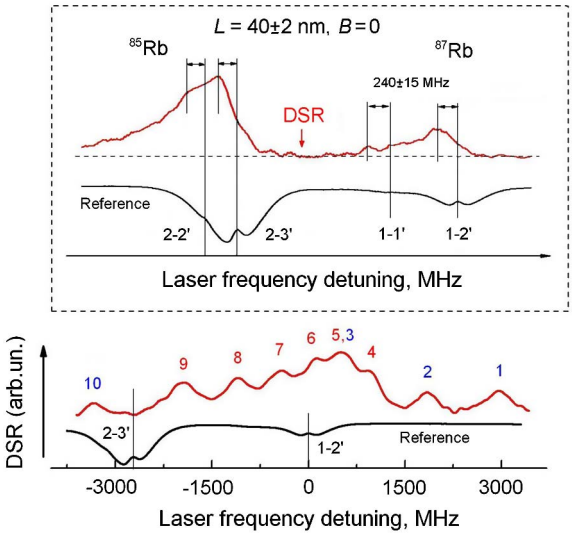

Fig. 4. Experimental DSR spectrum for $L = 40 \pm 2$ nm recorded at $B = 2.15$ kG (upper trace) and $B = 0$ reference spectrum (lower trace). Inset: DSR and reference spectra at $B = 0$ showing -240 ± 15 MHz red shift with respect to ^{87}Rb $F_g = 1 \rightarrow F_e = 1, 2$ and ^{85}Rb $F_g = 2 \rightarrow F_e = 2, 3$ reference frequencies.

and w2, respectively (in μm). The overall shift is depicted by curve 3, which is the sum of curves 1 and 2. For $L = 50$ nm, the recorded −130 MHz shift is obtained by taking vdW coefficient $C_3 = 1.0 \pm 0.1$ kHz × μm^3, which is consistent with the results of previous studies [7]. As is seen from the diagram, the maximum of the spectral density of an overall signal (the shifted peak) corresponds to the minimum value of the shift, so this value is estimated by the expression

$$\Delta\nu_{\mathrm{vdW}} = -2C_3/(L/2)^3. \quad \textbf{(1)}$$

To record SR signals above the noise level for an even smaller cell thickness $L = 40 \pm 2$ nm, the cell temperature was further increased to $T_R = 180$°C (vapor density $\sim 5 \times 10^{14}$ cm^{-3}). The DSR spectrum for this thickness and $B \approx 2.15$ kG is presented in Fig. 4. In these conditions, the transition peaks become broader, but the linewidth $\gamma_{\mathrm{DSR}} \approx$ 380 MHz still does not exceed a ∼500 MHz transition width obtained with a 1 mm long Rb cell [18]. It is noteworthy that the $F_g = 1 \rightarrow F_e = 1$ transition is prominent in the DSR spectrum, but hardly features in the reference trace. This illustrates the applied value of the method. An estimation of the number of atoms contributing to SR signal (Fig. 4) for a 0.5 mm beam diameter, $L = 40$ nm, and atomic density 5×10^{14} cm^{-3} gives $\sim 5 \times 10^6$. Note that the vdW shift for ^{85}Rb and ^{87}Rb transitions for the same L value is approximately equal.

Complete resolution of all the DSR peaks makes favorable the determination of a B-field, which can be done in two convenient ways: (1) by measuring the frequency shift of DSR peak 1 (ν_1) from the reference transition $F_g = 1 \rightarrow F_e = 2$ (see the inset of Fig. 5), also taking into account the value of vdW shift; and (2) by measuring the frequency separations between the individual transitions $a = \nu_{10} - \nu_1$ and $b = \nu_2 - \nu_1$, and exploiting the dependence of the a/b ratio on the B-field. Note that for case (2) there is no need for a frequency reference,

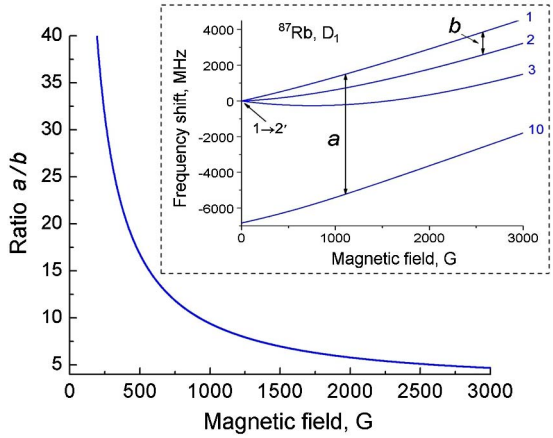

Fig. 5. B-field dependences of DSR frequencies exploited for the realization of two ways to determine the magnetic field value (see the text).

and the value of vdW shift is not important, being the same for all four transitions. Both B-field measurement techniques are graphically elucidated in Fig. 5.

The SR and DSR broadening observed with reduction of L and/or increase of T_R is caused by vdW interaction, as well as atom-window and atom-atom collisions. The measured DSR broadening γ_{DSR} versus L (cross marks) is presented in Fig. 6, along with fitted γ_{DSR}[MHz]≈15000/L[nm] dependence (dotted line). Note that the DRS broadening is mainly caused by the vdW interaction (the self-broadening rate resulting from the Rb–Rb collisions is ≈1 GHz/Torr, yielding much smaller contribution). Measuring magnetic field with nanometric-scale spatial resolution remains a challenge in a variety of problems, in particular when strong gradient fields are applied (e.g., 40 kG/mm in [19]). Even for $L = 25$ nm, γ_{DSR} is 600 MHz; thus, measuring the ratio a/b for a NC filled with a ^{87}Rb isotope, it is possible to determine the B-field value with the uniform ≈10 G precision over the 100–10,000 G range.

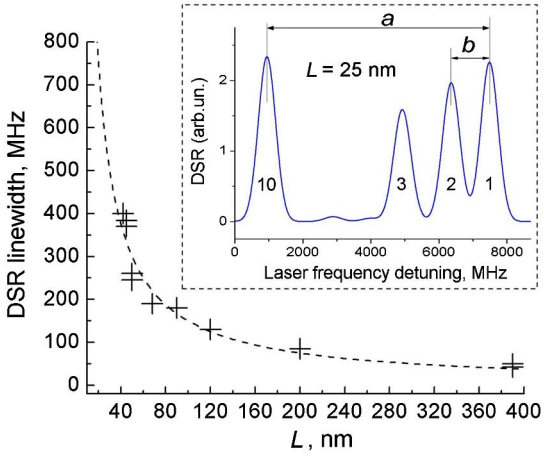

Fig. 6. Dependence of DSR linewidth γ_{DSR} versus L. Inset: four DSR peaks of the ^{87}Rb D_1 line at $L = 25$ nm and $B = 2$ kG; $\gamma_{\mathrm{DSR}} \approx 600$ MHz. The inset shows a theoretical spectrum calculated using dependences of the frequency shifts and transition probabilities versus a magnetic field; see [12].

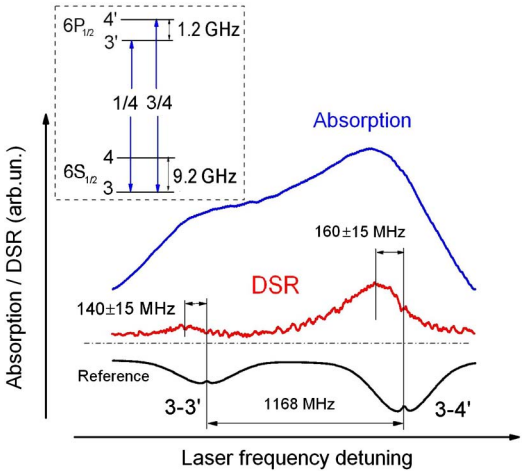

Fig. 7. Absorption spectrum (upper trace) and DSR spectrum (middle trace) recorded on Cs D_1 line and for $L \approx 52 \pm 3$ nm, $P_L \approx 0.2$ mW, NC temperature ≈170°C. The lower trace is the reference spectrum obtained with an auxiliary NC with $L = \lambda$, with VSOP resonances serving as ^{133}Cs $F_g = 3 \rightarrow F_e = 3, 4$ transition frequency markers [14]. The inset shows the diagram of these transitions with an indication of their relative intensities.

For comparison of the DSR with the absorption spectrum under the same conditions (for parameters, see the caption of Fig. 7), we have used $F_g = 3 \rightarrow F_e = 3.4$ transitions of Cs D_1 shown in the inset of Fig. 7. For this transition, the frequency separation of excited levels, ∼1.2 GHz, is the largest among the alkali metals. The latter is advantageous for avoiding the overlap of absorption lines of neighboring transitions. In Fig. 7, the upper curve shows the absorption spectrum for $L \approx 52$ nm, and the middle curve presents the DSR spectrum. The lowest line is the reference transmission spectrum obtained with an auxiliary NC with $L = \lambda$, exhibiting VSOP resonances at $F_g = 3 \rightarrow F_e = 3, 4$ transitions of ^{133}Cs [14]. The $F_g = 3 \rightarrow F_e = 3$ and $F_g = 3 \rightarrow F_e = 4$ transitions are strongly overlapped in the absorption spectrum, while DSR peaks for the same transitions are obviously advantageous: they are background-free, completely resolved, and exhibit noticeable frequency redshift (∼140 MHz and 160 MHz, respectively). An estimation of the C_3 vdW coefficient obtained from Eq. (1) gives $C_3 = 1.4 \pm 0.1$ kHz × μm^3.

The SR signal exhibits a low divergence, relatively high power (≈0.5% of the incident radiation), a linear response remaining up to $P_L \sim 5$ mW, and a high signal-to-noise ratio. Consequently, the DSR technique can be used for high-distance remote monitoring and mapping of both homogeneous and highly inhomogeneous B-fields in a wide range with ∼40 nm spatial resolution (for comparison with other types of magnetometers; see [20]). The DSR technique employing NCs is simple and easily realizable. We note that the recent development of a glass NC [21] can make this technique widely available, both for studies of atom-surface interaction and B-field mapping.

Funding. MES RA, Armenian State Committee of Science (SCS) (research projects nos. 15T-1C040, 15T-1C277).

Acknowledgment. The authors are grateful to A. Sarkisyan for the fabrication of nanocells, and to A. Tonoyan for theoretical calculations.

REFERENCES

1. R. W. Wood, Philos. Mag. **18**(103), 187 (1909).
2. J. P. Woerdman and M. F. H. Schuurmans, Opt. Commun. **14**, 248 (1975).
3. G. Nienhuis, F. Schuller, and M. Ducloy, Phys. Rev. A **38**, 5197 (1998).
4. A. Weis, V. A. Sautenkov, and T. W. Hänsch, Phys. Rev. A **45**, 7991 (1992).
5. H. Failache, S. Saltiel, M. Fichet, D. Bloch, and M. Ducloy, Phys. Rev. Lett. **83**, 5467 (1999).
6. I. Hamdi, P. Todorov, A. Yarovitski, G. Dutier, I. Maurin, S. Saltiel, Y. Li, A. Lezama, D. Sarkisyan, M. P. Gorza, M. Fichet, D. Bloch, and M. Ducloy, Laser Phys. **15**, 987 (2005).
7. D. Bloch and M. Ducloy, Adv. At. Mol. Opt. Phys. **50**, 91 (2005).
8. M. Fichet, G. Dutier, A. Yarovitsky, P. Todorov, I. Hamdi, I. Maurin, S. Saltiel, D. Sarkisyan, M. P. Gorza, D. Bloch, and M. Ducloy, Europhys. Lett. **77**, 54001 (2007).
9. K. A. Whittaker, J. Keaveney, I. G. Hughes, A. Sargsyan, D. Sarkisyan, and C. S. Adams, Phys. Rev. Lett. **112**, 253201 (2014).
10. E. A. Gazazyan, A. V. Papoyan, D. Sarkisyan, and A. Weis, Laser Phys. Lett. **4**, 801 (2007).
11. A. Sargsyan, E. Klinger, Y. Pashayan-Leroy, C. Leroy, A. Papoyan, and D. Sarkisyan, J. Exp. Theor. Phys. Lett. **104**, 224 (2016).
12. A. Sargsyan, E. Klinger, G. Hakhumyan, A. Tonoyan, A. Papoyan, C. Leroy, and D. Sarkisyan, J. Opt. Soc. Am. B **34**, 776 (2017).
13. D. Sarkisyan and A. Papoyan, in *New Trends in Quantum Coherence and Nonlinear Optics*, R. Drampyan, ed. (Nova Science, 2009), Chap. 3.
14. A. Sargsyan, G. Hakhumyan, R. Mirzoyan, and D. Sarkisyan, J. Exp. Theor. Phys. Lett. **98**, 441 (2013).
15. M. Zentile, J. Keaveney, L. Weller, D. J. Whiting, C. S. Adams, and I. G. Hughes, Comput. Phys. Commun. **189**, 162 (2015).
16. B. A. Olsen, B. Patton, Y. Y. Jau, and W. Happer, Phys. Rev. A **84**, 063410 (2011).
17. A. Sargsyan, G. Hakhumyan, C. Leroy, Y. Pashayan-Leroy, A. Papoyan, and D. Sarkisyan, Opt. Lett. **37**, 1379 (2012).
18. L. Weller, K. Kleinbach, M. Zentile, S. Knappe, I. G. Hughes, and C. S. Adams, Opt. Lett. **37**, 3405 (2012).
19. R. Folman, P. Kruger, J. G. Schmiemayer, J. Denschlag, and C. Henkel, Adv. At. Mol. Opt. Phys. **48**, 263 (2002).
20. D. Budker and D. F. J. Kimball, eds., *Optical Magnetometry* (Cambridge University, 2013), p. 432.
21. K. A. Whittaker, J. Keaveney, I. G. Hughes, A. Sargysyan, D. Sarkisyan, B. Gmeiner, V. Sandoghdar, and C. S. Adams, J. Phys. Conf. Ser. **635**, 122006 (2015).